

Strain-modulated Valley Polarization and Piezomagnetic Effects in Altermagnetic Cr_2S_2

Chen Chen,¹ Xiaoyang He,¹ Qizhen Xiong,² Chuye Quan,³
Haojie Hou,¹ Shilei Ji,^{1,*} Jianping Yang,¹ and Xing'ao Li^{1,3,4,†}

¹*School of Science, Nanjing University of Posts and Telecommunications (NJUPT), Nanjing 210023, China.*

²*The Faculty of Mathematical & Physical Sciences,
University College London(UCL), London WC1E6BT, England.*

³*Institute of Advanced Materials (IAM), Nanjing University of
Posts and Telecommunications (NJUPT), Nanjing 210023, China.*

⁴*College of science, Zhejiang University of Science and Technology, Hangzhou 310023, China.*

(Dated: October 24, 2024)

Altermagnetism exhibits advantages over both ferromagnetic and antiferromagnetic counterparts by enabling spin splitting within antiferromagnetic materials. Currently, it is established that valley polarization in altermagnetism remains largely insensitive to spin-orbit coupling and spin. Here, using Cr_2S_2 as a case study, we investigate the mechanism through which an external field modulates valley polarization in altermagnetism. This effect arises from the external field's disruption of diagonal mirror symmetry M_{xy} , consequently inducing valley polarization within the material. Strain not only induces valley polarization but also generates an almost uniform magnetic field, which can reach as high as 118.39 T under 5% uniaxial strain. In addition, this symmetry breaking in Cr_2S_2 monolayers results in significant piezomagnetic properties, merging piezomagnetic and altermagnetic characteristics in two-dimensional materials.

I. INTRODUCTION

With continuous advancements in science and technology, magnetic materials are playing an increasingly important role in scientific research.[1–3] Recently, a new type of magnetism called ‘altermagnetism’ has garnered significant attention as a third category distinct from traditional ferromagnetism (FM) and antiferromagnetism (AFM).[4, 5] Current research in spintronics primarily focuses on exploring transport and quantum states dominated by FM.[6–8] However, FM is susceptible to external interference, causing magnetic instability. AFM, characterized by magnetic field stability and ultrafast dynamics[9–11], maintains zero magnetic moment and PT symmetry. Altermagnets have dual properties similar to ferromagnets and antiferromagnets. On one hand, like AFM, altermagnets possess a zero magnetic moment and are resistant to external magnetic field interference. On the other hand, similar to FM, the spin-dependent bands of the altermagnet also split at the K point, and the band splitting is spread throughout the k space, resulting in FM related quantum transport characteristics. This discovery not only advances spintronics research but also provides new insights into potential superconducting states in various magnetic materials.[12, 13] Several two-dimensional materials have been predicted to exhibit altermagnetism, such as RuO_2 [14], MnTe [15], and Cr_2SO [16].

The integration of charge and spin degrees of freedom with valley degrees of freedom[6, 17] in ferrovalley mate-

rials has emerged as a prominent research focus in valleytronics, holding significant promise for encoding, manipulating, and transmitting information.[18–20] Recent experiments have spotlighted two-dimensional transition-metal dichalcogenides (TMDCs)[21–23] with strong spin-orbit coupling (SOC) in the realm of valley electronics. In TMDCs, valley polarization is absent owing to time reversal symmetry protection. Various approaches have been explored to induce valley polarization, including optical pumping[24–26], magnetic doping[27, 28], external magnetic fields[29, 30], and magnetic proximity[31] have been explored. Recently, ferrovalley two-dimensional materials with intrinsic valley polarization have been proposed.[22, 32] Importantly, altermagnetic candidates are particularly appealing for valley electronics applications due to their high storage density, resilience to external magnetic fields, and ultra-fast write speeds.[33–35]

To assess the electromagnetic characteristics of materials, we focus on the piezomagnetic effect. Traditional piezomagnetism refers to the phenomenon wherein the application of an external magnetic field alters the internal magnetization of a magnetic material.[36, 37] Instead of rearranging the magnetic moments inside the material, the piezomagnetism here is caused by a strain-induced occupation imbalance between spin-up and spin-down electrons, which is mainly determined by the anisotropy of electronic properties.[38, 39]

In this paper, we predict Cr_2S_2 is a 2D altermagnetic material and provide a detailed analysis of the mechanisms by which an external field modulates valley polarization in such materials, using Cr_2S_2 as a case study. Cr_2S_2 monolayer with spatial symmetry group $P4 - mmm$ is proposed based on first principles, and its stability, magnetic ground state, band structure and magnetic anisotropy are investigated in detail. Cr_2S_2

* njuptjishilei@outlook.com

† lxahbmy@126.com

monolayers exhibit AFM semiconductor properties with in-plane magnetic anisotropy character. We observe the generation of an almost uniform effective magnetic field under strain conditions, achieving a strength of 118.39 T when the uniaxial strain is 5%. Interestingly, the Cr₂S₂ monolayer has piezomagnetic properties. The magnetization size and direction can be adjusted by electron doping concentration and uniaxial strain strength. It provides a platform for the application of spin device. It is important to highlight that under biaxial tensile strain, the Cr₂S₂ monolayer fails to achieve valley polarization and piezomagnetic properties due to the inability of biaxial strain to alter the M_{xy} symmetry of the crystal. This is because the biaxial strain does not change the M_{xy} symmetry of the crystal.

II. COMPUTATIONAL DETAILS

Within the framework of density functional theory (DFT), we perform spin-polarized first-principles calculations using the standard VASP code and the projector augmented-wave (PAW) method.[40–42] We employ the generalized gradient approximation of Perdew-Burke-Ernzerhof (PBE-GGA) as the exchange-correlation functional.[43] The kinetic energy cutoff is set to 500 eV, total energy convergence criterion of 10^{-8} eV, and force convergence criterion of 0.0001 eV/Å. To describe Cr 3d electrons, the field coulomb of Cr 3d electrons is set to $U = 2.26$ eV.[44, 45] A vacuum space of more than 20 Å is imposed to avoid interlayer interactions. A $14 \times 14 \times 1$ Monkhorst-Pack k-point is employed to sample the first Brillouin zone. The SOC effect is considered to study the band structure and magnetocrystalline anisotropy of the Cr₂S₂ monolayer under strain. The Phonon dispersion spectrum of Cr₂S₂ monolayers is obtained using the PHONOPY code with a $2 \times 2 \times 1$ supercell.[46]

III. RESULTS AND DISCUSSION

A. STRAIN-MODULATED VALLEY POLARIZATION

We analyze the mechanism by which uniaxial strain modulates valley polarisation and explain why biaxial strain fails to induce valley polarisation. The energy gain at the extreme valley (assuming non-degenerate) is[38]

$$\Delta E = \sum_{ij} d_{ij} \varepsilon_{ij}, \quad (1)$$

where d is the tensor of deformation potential and ε is the strain tensor. The $i, j \in x, y$. The diagonal mirror symmetry M_{xy} is expressed as

$$M_{xy} = \begin{pmatrix} 0 & -1 \\ -1 & 0 \end{pmatrix}. \quad (2)$$

Under external strain, the energy displacement of valley X is

$$\Delta E_X = d_{xx} \varepsilon_{xx} + d_{yy} \varepsilon_{yy} + 2d_{xy} \varepsilon_{xy}, \quad (3)$$

and the energy displacement of valley Y can be calculated as

$$\Delta E_Y = d_{yy} \varepsilon_{xx} + d_{xx} \varepsilon_{yy} + 2d_{xy} \varepsilon_{xy}. \quad (4)$$

The energy displacement of the X and Y valleys under uniaxial strain along the X axis is

$$\begin{aligned} \Delta E_X &= d_{xx} \varepsilon_{xx} \\ \Delta E_Y &= d_{yy} \varepsilon_{xx}, \end{aligned} \quad (5)$$

then the relative energy displacement of the two valleys is

$$\delta E^{V/C} = \Delta E_X^{V/C} - \Delta E_Y^{V/C} = \eta^{V/C} \varepsilon_{xx}, \quad (6)$$

where $\delta E^{V/C}$ is the size of valley splitting of conduction and valence band, $\eta^{V/C} = (d_{xx} - d_{yy})$ is a constant. The mirror symmetry M_{xy} is broken due to the presence of uniaxial strain ε_{xx} , which leads to the emergence of valley polarization. According to Equation(6), the relationship between valley splitting size and strain strength is linear. By fitting Fig. 4(a), we get $\eta^V = -18.46$, $\eta^C = 12.22$. The energy displacement of X and Y valleys under biaxial strain is

$$\Delta E_X = \Delta E_Y = 2d_{xy} \varepsilon_{xy}, \quad (7)$$

then the relative energy displacement of the two valleys is

$$\delta E^{V/C} = 0, \quad (8)$$

this indicates that biaxial strain does not produce valley splitting, consistent with the results in Fig. 4(b).

B. ATOMIC AND MAGNETIC STRUCTURES

Figs. 1(a) and (b) illustrate the crystal structure of a Cr₂S₂ monolayer, which has three atomic layers, the middle layer is composed of Cr atoms, and the upper and lower layers are S atoms. Each Cr atom is surrounded by four S atoms, and the unit cell of monolayer Cr₂S₂ consists of two Cr atoms and two S atoms. The optimized lattice constants for the Cr₂S₂ monolayer is 3.783 Å. The magnetic moments of the two Cr atoms are 3.404 μ_B and -3.404 μ_B , respectively, resulting in a total magnetic moment of 0.00 μ_B . The monolayer Cr₂S₂ possesses a square lattice structure, and its symmetry is described by the space symmetry group $P4 - mmm$, which is a simple space group of the point group D_{4h} .

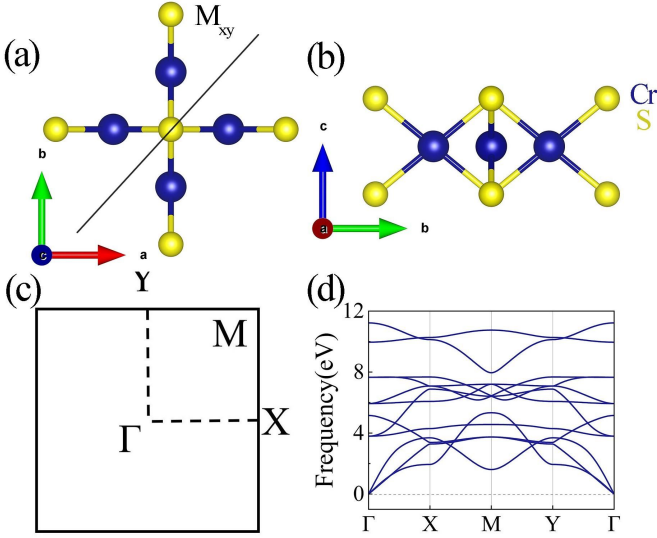


FIG. 1. Lattice and phonon spectrum of Cr_2S_2 monolayer (a) and (b) Top view and side view of Cr_2S_2 monolayer, where the balls of dark blue and yellow label the Cr and S atoms, respectively. (c) The first Brillouin zone with high symmetry points. (d) Phonon spectrums of monolayer Cr_2S_2 .

TABLE I. The energy difference between Néel AFM and FM, zigzag AFM and stripy AFM configurations, where AFM1 represents Néel AFM, AFM2 represents zigzag AFM, and AFM3 represents stripy AFM

$E_{\text{FM-AFM1}}$	$E_{\text{AFM2-AFM1}}$	$E_{\text{AFM3-AFM1}}$
960.3 meV	283.5 meV	370.5 meV

The D_{4h} point group contains C_4^Z , C_2^X and I . The Brillouin zone for the band structure calculation is shown in Fig. 1(c), which is related to the crystal structure. To illustrate the stability of Cr_2S_2 , phonon dispersion calculations are performed. By calculating the phonon dispersion of the $2 \times 2 \times 1$ supercell, the dynamic stability of the structure is confirmed, as illustrated in Fig. 1(d). Notably, no virtual frequencies are observed in the phonon spectrum, indicating that Cr_2S_2 is dynamically stable. As mentioned previously, altermagnetism is a combination of AFM and FM. We constructed FM and AFM structures using $2 \times 2 \times 1$ supercells to determine the antiferromagnetic properties of the Cr_2S_2 monolayer. As shown in Fig. 2, we investigate one FM and three AFM structures. The energies of FM and Néel AFM, zigzag AFM and stripy AFM configurations are listed in Table I. It is proved that the energy of Néel AFM per unit cell is 960.3 meV, 283.5 meV and 370.5 meV lower than those of FM, zigzag AFM and stripy AFM cases. This confirms the Néel AFM configuration for the Cr_2S_2 monolayer.

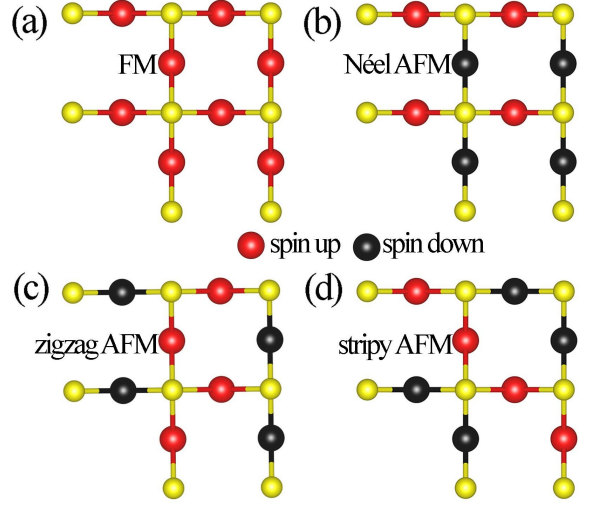


FIG. 2. (a) FM, (b) Néel AFM, (c) zigzag AFM and (d) stripy AFM configurations of the Cr_2S_2 monolayer. Red and black balls indicate spin-up and spin-down directions, respectively.

C. ELECTRONIC STRUCTURES

After confirming the AFM ground state of the Cr_2S_2 monolayer, we further investigate the band structure of the Cr_2S_2 monolayer. The band structure of the Cr_2S_2 monolayer without considering SOC is shown in Fig. 3(a). There are two valleys at the X and Y points, and the states near these points mainly originate from two different Cr atoms. Unlike the general band structure of AFM[47], the band structure of the Cr_2S_2 shows spin-splitting phenomenon. In Cr_2S_2 , the two sublattices Cr1-S and Cr2-S have different orientations, one in the x direction and the other in the y direction in Fig. 1(a). The two sublattices are symmetrically M_{xy} related by diagonal mirrors, which produces spin splitting. For the unstrained case, the gap between the X and Y valleys is the same, indicating that there is no valley polarization. Compared to Cr_2O_2 [44] without considering SOC, it can be clearly observed that there is no longer Weyl cones in the Cr_2S_2 band structure. This is because the onsite energy of S and O are different. Moreover, Cr_2S_2 is a direct band gap semiconductor with a gap value of 0.639 eV. The conductor band minimum (CBM) and the valence band maximum (VBM) of Cr_2S_2 come from bands with different spin directions. The Cr atom is affected by a crystal field with D_{4h} symmetry, and the original five-fold degeneracy of the 3d orbitals is lifted and split into four groups: a non-degenerate A1 (d_{z^2}) orbital, two non-degenerate B1 ($d_{x^2-y^2}$) and B2 (d_{xy}) orbitals, and a doubly degenerate E (d_{xz} , d_{yz}) orbital. As shown in Fig. 3(b), the VBM mainly comes from the d_{xy} orbitals, while the CBM comes from the d_{z^2} and $d_{x^2-y^2}$ orbitals.

To obtain valley polarization in Cr_2S_2 , it is necessary to break the diagonal mirror symmetry M_{xy} . Strain engineering has been widely used to modulate the band

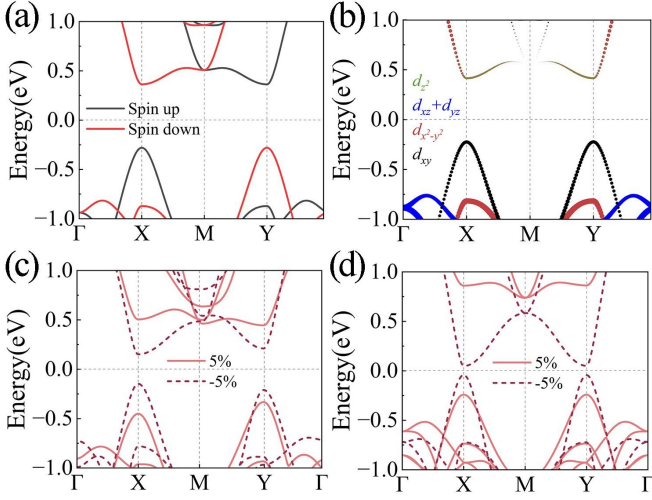


FIG. 3. Band structures of monolayer Cr₂S₂. (a) Band structures without considering SOC. (b) The projected PBE band structures for the Cr₂S₂ monolayers. Band structure evolution under different (c) strains along x direction (-5%, 5%) and (d) biaxial strain (-5%, 5%).

structure of two-dimensional materials[48], and the symmetry of two-dimensional materials can be changed by applying uniaxial strain. Therefore, we apply uniaxial strain to adjust the band structure, which breaks the M_{xy} symmetry so that the rotational symmetry C_4 is reduced to C_2 . Strain (ε) is defined as $(a-a_0)/a_0$. Here, a and a_0 are lattice constants in the presence and absence of strain. Fig. 3(c) shows the band structure of a Cr₂S₂ monolayer considering uniaxial compressive and tensile strains. Compared to the unstrained case, the X, Y valleys still exist, but the energies at these valleys are not equal, breaking their degeneracy. For a strain of 5%, the band gap of the X valley energy decreases, while the band gap of the Y valley energy increases, resulting in a large valley polarization of the Cr₂S₂ monolayer. Valley polarization is defined as $\Delta E_{V(C)} = E_{V(C)}^Y - E_{V(C)}^X$. The valley polarization generated by the valence band, denoted as $\Delta E_V = -118.39 \text{ meV}$ and the valley polarization $\Delta E_C = 59.81 \text{ meV}$ in the conduction band, sum up to a total valley polarization of $\Delta E_{VCP} = 178.20 \text{ meV}$ ($\Delta E_{VCP} = \Delta E_C - \Delta E_V$). The valley splitting of the Cr₂S₂ is higher than the valley splittings of many widely studied ferromagnetic materials.[48–50]

Compared with 5%, the valley polarization reverses when the strain is -5%. Meanwhile, the strain in the opposite direction produces the exact opposite valley polarization, the VBM and the CBM are both in the Y valley. From compressive to tensile strain, the band structure further away from the Fermi level. The coupling property between valley polarization and strain direction allows us to use strain control valley and apply it to logic devices, which can be applied to logic devices. In addition, we also exhibit the change of band structure under biaxial strain. As delivered Fig. 3(d), Under 5%

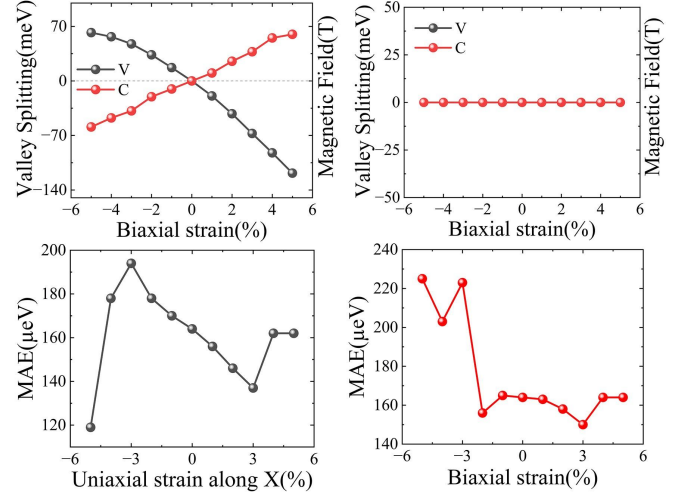


FIG. 4. Variations in band structure, effective magnetic field, and MAE under strain. The changes in valley polarization of the valence band and conduction band of the Cr₂S₂ monolayer are presented for (a) uniaxial strain along the X direction and (b) biaxial strain, along with the corresponding variations in the effective magnetic field. MAE under different (c) uniaxial strains along X and (d) biaxial strain. The strain range is -5% to 5%.

and -5% biaxial strain, the energies of the X and Y valleys are equal, resulting in no valley polarization. This is because biaxial strain does not break the diagonal mirror symmetry M_{xy} .

The evolution of valley splitting under strain are plotted in Fig. 4(a) and (b). Consistent with the above analysis, uniaxial strain can induce valley polarization. And with the increase of compressive and tensile strength, valley splitting also increases, which is conducive to the experimental manipulation of these valleys. In the case of biaxial strain, no matter how we regulate the strain, there will be no valley polarization. The specific changes in the band structure under strain are shown in Figures S2 and S3. In summary, symmetry breaking is the key to valley polarization of altermagnet.

It can also be observed from Fig. 3(c) that the conduction band (valence band) around the X (Y) valley has almost the same energy displacement under the action of uniaxial strain, indicating that the uniaxial strain induces a static and uniform effective magnetic field. The strength of the induced effective magnetic field can be expressed as[51]

$$B_{c(v)}^{\text{eff}} \equiv \frac{\delta E^{V/C}}{g_s s_z}, \quad (9)$$

where $\delta E^{V/C}$ is the size of valley splitting of conduction and valence band, $g_s = 1/2$, $s_z = 2$. Equation(9) can be expressed as follows:

$$B_{c(v)}^{\text{eff}} = \delta E^{V/C} = \eta^{V/C} \varepsilon_{xx}. \quad (10)$$

The variation of the effective magnetic field is consistent

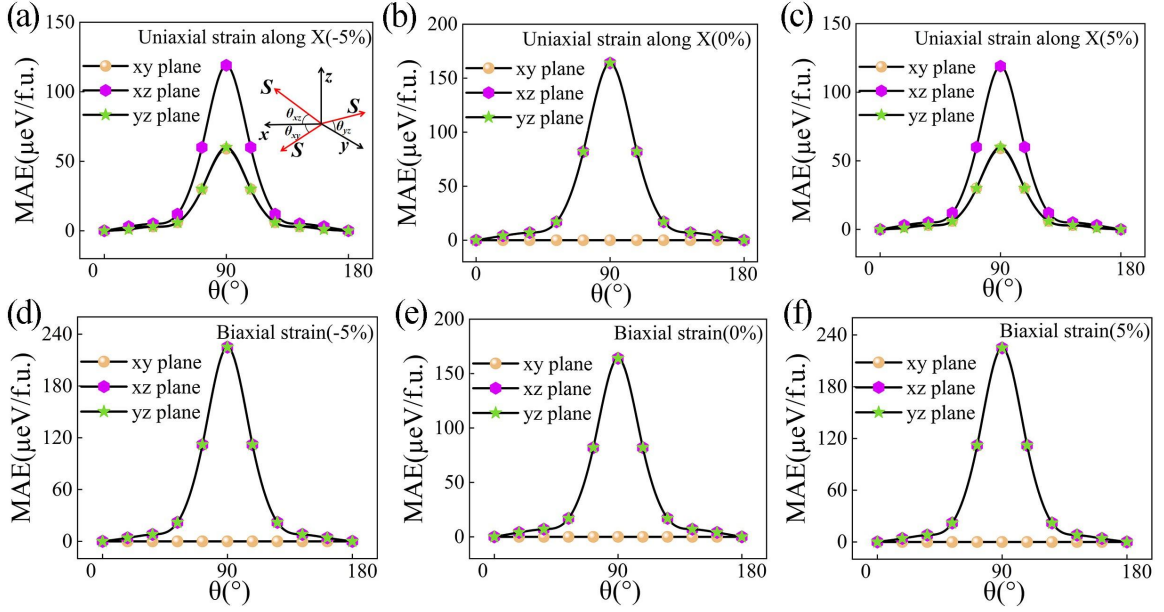


FIG. 5. MAE of the Cr_2S_2 monolayers along xy, xz and yz planes. Under different (a–c) uniaxial strains along x direction (–5%, 0%, and 5%) and (d–f) biaxial strains (–5%, 0%, and 5%).

with Equation(6). As shown in Fig. 4(a), the effective magnetic field $B_{c(v)}^{\text{eff}}$ and the valley splitting δE exhibit the same trend under uniaxial strain. With a 5% uniaxial strain, effective magnetic fields $B_v^{\text{eff}} = 118.39\text{T}$ and $B_c^{\text{eff}} = 59.81\text{T}$ are produced. This indicates that the altermagnetic materials can generate an effective magnetic field under small strains.

Magnetic anisotropy energy(MAE) is one of the key factors to realize long–range magnetic order in two-dimensional materials, which is directly related to the thermal stability of magnetic data storage. MAE is represented as $MAE = E[001] - E[100]$, where $E[100]$ and $E[001]$ are the system energies when the magnetic moment is along the in–plane $[100]$ axis and the out-of-plane $[001]$, respectively. In this study, we used $GGA+U+SOC$ method to calculate the total energy in the direction of magnetic moment $[100]$, $[001]$. The MAE value of the Cr_2S_2 monolayer is -0.164meV , with $E[100] - E[001] < 0$, indicating in–plane magnetic anisotropy (IMA) character. Fig. 4(c) and (d) demonstrates the effects of uniaxial and biaxial strains on MAE. The Cr_2S_2 monolayer maintains IMA behavior throughout the strain range, this shows the robustness of MAE under strain.

To further analyze the characteristics of MAE in the whole space, we calculate the projection of MAE on the xy, xz and yz planes, as observed in Fig. 5. It is clear that MAE exhibits a strong dependence on the direction of magnetization along the xz and yz planes, independent of the xy planes in Fig. 5(b).and Fig. 5(e). When uniaxial strain is applied, it changes the rotational symmetry from C_4 to C_2 , leading to symmetry breaking. At this point, the MAE is anisotropic in the xy, xz, and yz planes. This phenomenon does not occur un-

der biaxial strain. The MAE remains isotropic in the xy plane and anisotropic in the xz and yz planes. This is because biaxial strain does not change the symmetry, and the rotational symmetry remains as C_4 . From Figure S4 and Figure S5, it can be seen that the contribution of the Cr-p orbitals is relatively small, an order of magnitude less than that of the d orbitals. As the compressive strain increases, the contribution of d_{z^2} and d_{yz} hybridization to the anisotropy in the $[010]$ direction decreases, while the contribution of d_{z^2} and d_{xy} hybridization to the anisotropy in the $[100]$ direction also decreases. Overall, under compressive strain, the reduction in the contribution of Cr’s d orbitals along the $[100]$ direction is greater than that along the $[010]$ direction. This disparity results in the emergence of anisotropy in the xy plane under uniaxial strain conditions.

D. PIEZOMAGNETISM IN MONOLAYER

As mentioned above, Cr_2S_2 monolayer can easily generate valley polarization using uniaxial strain, which provides new opportunities to generate net magnetization. Piezomagnetic is generated by the inherent magnetoelastic coupling, which is a static property. This coupling can also lead to magnetostriction where one can induce a strain using an external magnetic field. Strain-induced magnetization is obtained as[38]:

$$M(\theta, \varepsilon_\theta, n) = \begin{cases} -\gamma_{\phi\theta}\varepsilon_\theta, & 0 \leq \varepsilon_\theta < \frac{n}{|\gamma_{\phi\theta}|}, \\ -\text{sign}(\gamma_{\phi\theta})n, & \varepsilon_\theta \geq \frac{n}{|\gamma_{\phi\theta}|} \end{cases}, \quad (11)$$

where $\gamma_{\phi\theta} = \rho[(D_{xx} - D_{yy})\sin 2\phi - 2D_{xy}\cos 2\phi]\sin(2\phi - 2\theta) = \gamma\sin(2\phi - 2\theta)$, γ is a constant, ϕ is the angle

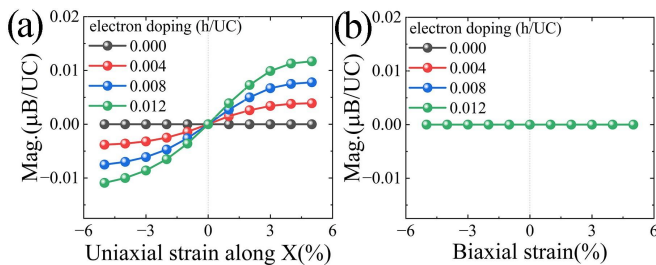


FIG. 6. Strain-induced piezomagnetic in electron-doped monolayer Cr_2S_2 . The net magnetization change under (a) uniaxial strains along X and (b) biaxial strains.

between the mirror and the X-axis, θ is the angle between the direction of uniaxial strain applied and the X-axis. In this paper, $\phi = \pi/4$, $\theta = 0$. Uniaxial strain-induced magnetization is obtained as can be written as

$$M = \begin{cases} -\gamma\varepsilon, & 0 \leq \varepsilon < \frac{n}{|\gamma|}, \\ -\text{sign}(\gamma)n, & \varepsilon \geq \frac{n}{|\gamma|}, \end{cases} \quad (12)$$

according to the Equation(12), the relationship between magnetization and strain is linear under finite strain. With the increase of strain, the magnetization becomes saturated. Similarly, the biaxial strain magnetisation M is 0. To accurately determine the magnetization during electron doping, we tested the K-point convergence, as illustrated in Figure S6. Fig. 6(a) displays the magnetization in relation to carriers density and uniaxial strain. The magnetization increases with both carrier density and strain, and the direction of magnetization is indeed reversed for tensile and compressive strains. In the absence of strain, there is no net magnetic moment because. This is because the diagonal mirror symmetry M_{xy} is preserved. When the strain is small, the magnetization increases linearly with the strain, which is consistent with the description of Equation(12). As the strain strength increases gradually, the magnetization tends to be saturated. This is consistent with our previous analysis. One can see from Fig. 6(b) that since the symmetry is not broken, the biaxial strain does not change the magnetization and remains zero. Compared with the piezomagnetism in nonlinear antiferromagnetic materials[37], the piezomagnetism of Cr_2S_2 is much larger, and there are

ways to adjust the size and direction of magnetization. Given a strain intensity, the magnetization magnitude can be adjusted by the electron doping concentration. Given the electron doping concentration, the direction of magnetization can be changed by uniaxial strain. The piezomagnetic properties of Cr_2S_2 make it a good candidate for magnetic sensors and other applications.

IV. CONCLUSION

In summary, we investigate the influence of external field modulation on valley polarization. Utilizing DFT calculations, we systematically examine several properties of the Cr_2S_2 monolayer, including its stability, magnetic ground state, band structure, and magnetic anisotropy. The Cr_2S_2 monolayer demonstrates excellent stability with an AFM magnetic ground state and intriguing spin valley splitting, establishing it as an altermagnetic material. Valley polarization can be manipulated through uniaxial strain, with the direction of polarization altered by varying between compressive and tensile strains. However, such polarization control is absent under biaxial strains, which maintain the diagonal mirror symmetry M_{xy} and preserve the C_4 rotational symmetry. We find that an almost uniform effective magnetic field is generated under uniaxial strain, which provides favorable conditions for applications in spintronic strain control. The MAE of Cr_2S_2 monolayers remains robust and in-plane under both uniaxial and biaxial strains. Further analysis of MAE in the whole space shows that MAE is isotropic in the xy plane under the absence of strain and biaxial strain. However, under uniaxial strain, MAE exhibits anisotropy in xy, zx and yz planes. Remarkably, under the influence of uniaxial strain, the Cr_2S_2 monolayer exhibits piezomagnetic characteristics. Modulating hole doping and adjusting strain strength allow precise control over the size and orientation of magnetization. Our findings contribute to the advancement of altermagnetic and valleytronic materials, promising significant potential for energy-efficient and ultra-fast valleytronic devices.

We acknowledge the fundings from National Natural Science Foundation of China (Grant No. 51872145), Postgraduate Research & Practice Innovation Program of Jiangsu Province (Grant No. KYCX23_0977), and Qinglan Project of Jiangsu Province of China.

-
- [1] P. Man, L. Huang, J. Zhao, and T. H. Ly, Ferroic phases in two-dimensional materials, *Chem. Rev.* **123**, 10990 (2023).
 - [2] R. Oja, K. Johnston, J. Frantti, and R. M. Nieminen, Computational study of (111) epitaxially strained ferroelectric perovskites BaTiO_3 and PbTiO_3 , *Phys. Rev. B* **78**, 094102 (2008).
 - [3] Q. Pei, B. Zhou, W. Mi, and Y. Cheng, Triferroic ma-

- terial and electrical control of valley degree of freedom, *ACS Appl. Mater. Interfaces* **11**, 12675 (2019).
- [4] L. Šmejkal, J. Sinova, and T. Jungwirth, Beyond conventional ferromagnetism and antiferromagnetism: A phase with nonrelativistic spin and crystal rotation symmetry, *Phys. Rev. X* **12**, 031042 (2022).
- [5] I. I. Mazin, Altermagnetism in mnTe: Origin, predicted manifestations, and routes to detwinning, *Phys. Rev. B*

- 107**, L100418 (2023).
- [6] H. Hu, W. Y. Tong, Y. H. Shen, X. Wan, and C. G. Duan, Concepts of the half-valley-metal and quantum anomalous valley hall effect, *NPJ Comput. Mater* **6**, 129 (2020).
 - [7] W. Xie, L. Zhang, Y. Yue, M. Li, and H. Wang, Giant valley polarization and perpendicular magnetocrystalline anisotropy energy in monolayer MX_2 ($M = \text{Ru, Os}$; $X = \text{Cl, Br}$), *Phys. Rev. B* **109**, 024406 (2024).
 - [8] K. Jia, X.-J. Dong, S.-S. Li, W.-X. Ji, and C.-W. Zhang, Spontaneous valley polarization and valley-nonequilibrium quantum anomalous hall effect in janus monolayer scbri, *Nanoscale* **15**, 8395 (2023).
 - [9] H. T. Hirose, J.-i. Yamaura, and Z. Hiroi, Robust ferromagnetism carried by antiferromagnetic domain walls, *Sci. Rep* **7**, 42440 (2017).
 - [10] X. Hu, Half-metallic antiferromagnet as a prospective material for spintronics, *Adv. Mater* **24**, 294 (2012).
 - [11] T. Jungwirth, J. Sinova, A. Manchon, X. Marti, J. Wunderlich, and C. Felser, The multiple directions of antiferromagnetic spintronics, *Nat. Phys* **14**, 200 (2018).
 - [12] S. Reimers, L. Odenbreit, L. Smejkal, V. N. Strocov, P. Constantinou, A. B. Hellenes, R. J. Ubierto, W. H. Campos, V. K. Bharadwaj, A. Chakraborty, T. Denneulin, W. Shi, R. E. Dunin-Borkowski, S. Das, M. Klauui, J. Sinova, and M. Jourdan, Direct observation of altermagnetic band splitting in CrSb thin films, *Nat. Commun* **15**, 2116 (2024).
 - [13] L. Šmejkal, A. B. Hellenes, R. González-Hernández, J. Sinova, and T. Jungwirth, Giant and tunneling magnetoresistance in unconventional collinear antiferromagnets with nonrelativistic spin-momentum coupling, *Phys. Rev. X* **12**, 011028 (2022).
 - [14] S. W. Lovesey, D. D. Khalyavin, and G. van der Laan, Magnetic structure of RuO₂ in view of altermagnetism, *Phys. Rev. B* **108**, L121103 (2023).
 - [15] T. Osumi, S. Souma, T. Aoyama, K. Yamauchi, A. Honma, K. Nakayama, T. Takahashi, K. Ohgushi, and T. Sato, Observation of a giant band splitting in altermagnetic MnTe, *Phys. Rev. B* **109**, 115102 (2024).
 - [16] S. D. Guo, X. S. Guo, K. Cheng, K. Wang, and Y. S. Ang, Piezoelectric altermagnetism and spin-valley polarization in Janus monolayer Cr₂SO, *Appl. Phys. Lett* **123**, 082401 (2023).
 - [17] J. Chu, Y. Wang, X. Wang, K. Hu, G. Rao, C. Gong, C. Wu, H. Hong, X. Wang, K. Liu, C. Gao, and J. Xiong, 2D Polarized Materials: Ferromagnetic, Ferrovalley, Ferroelectric Materials, and Related Heterostructures, *Adv. Mater* **33**, 2004469 (2021).
 - [18] A. Ciarrocchi, F. Tagarelli, A. Avsar, and A. Kis, Excitonic devices with van der waals heterostructures: valleytronics meets twistronics, *Nat. Rev. Mater* **7**, 449 (2022).
 - [19] K. F. Mak, K. L. McGill, J. Park, and P. L. McEuen, Valleytronics. The valley Hall effect in MoS₂ transistors, *Science* **344**, 1489 (2014).
 - [20] Y. Tan, J. Zheng, X. Niu, Y. Zhao, N. Zhong, B. Tian, and C. Duan, Research progress on 2D ferroelectric and ferrovalley materials and their neuromorphic application, *Sci. China Phys. Mech. Astron* **66**, 1674 (2023).
 - [21] D. MacNeill, C. Heikes, K. F. Mak, Z. Anderson, A. Kormányos, V. Zólyomi, J. Park, and D. C. Ralph, Breaking of Valley Degeneracy by Magnetic Field in Monolayer MoSe₂, *Phys. Rev. Lett.* **114**, 037401 (2015).
 - [22] W. Y. Tong, S. J. Gong, X. Wan, and C. G. Duan, Concepts of ferrovalley material and anomalous valley hall effect, *Nat. Commun* **7**, 13612 (2016).
 - [23] D. Xiao, G.-B. Liu, W. Feng, X. Xu, and W. Yao, Coupled Spin and Valley Physics in Monolayers of MoS₂ and Other Group-VI Dichalcogenides, *Phys. Rev. Lett.* **108**, 196802 (2012).
 - [24] W. Yao, D. Xiao, and Q. Niu, Valley-dependent optoelectronics from inversion symmetry breaking, *Phys. Rev. B* **77**, 235406 (2008).
 - [25] H. Zeng, J. Dai, W. Yao, D. Xiao, and X. Cui, Valley polarization in MoS₂ monolayers by optical pumping, *Nat. Nanotechnol* **7**, 490 (2012).
 - [26] K. F. Mak, K. He, J. Shan, and T. F. Heinz, Control of valley polarization in monolayer MoS₂ by optical helicity, *Nat. Nanotechnol* **7**, 494 (2012).
 - [27] J. E. H. Braz, B. Amorim, and E. V. Castro, Valley-polarized magnetic state in hole-doped monolayers of transition-metal dichalcogenides, *Phys. Rev. B* **98**, 161406 (2018).
 - [28] N. Singh and U. Schwingenschlögl, A Route to Permanent Valley Polarization in Monolayer MoS₂, *Adv. Mater* **29**, 1600970 (2017).
 - [29] C. Lei, X. Li, Y. Ma, and Z. Qian, Reversible nonvolatile control of anomalous valley hall effect in a multiferroic van der waals heterostructure, *Phys. Rev. B* **108**, 155431 (2023).
 - [30] T. Zhang, X. Xu, B. Huang, Y. Dai, L. Kou, and Y. Ma, Layer-polarized anomalous hall effect in valleytronic van der waals bilayers, *Mater. Horiz* **10**, 483 (2023).
 - [31] T. Norden, C. Zhao, P. Zhang, R. Sabirianov, A. Petrou, and H. Zeng, Giant valley splitting in monolayer WS₂ by magnetic proximity effect, *Nat. Commun* **10**, 4163 (2019).
 - [32] X. Feng, X. Xu, Z. He, R. Peng, Y. Dai, B. Huang, and Y. Ma, Valley-related multiple Hall effect in monolayer VS₂P₄, *Phys. Rev. B* **104**, 075421 (2021).
 - [33] S. D. Guo, Y. L. Tao, Z. Y. Zhuo, G. Zhu, and Y. S. Ang, Electric-field-tuned anomalous valley Hall effect in A-type hexagonal antiferromagnetic monolayers, *Phys. Rev. B* **109**, 134402 (2024).
 - [34] Y. Xu, H. Liu, Y. Dai, B. Huang, and W. Wei, Spin-valley splitting and spontaneous valley polarization in antiferromagnetic Mn₂P₂X₃Y₃ monolayers, *Appl. Phys. Lett* **122**, 242404 (2023).
 - [35] S. D. Guo, W. Xu, Y. Xue, G. Zhu, and Y. S. Ang, Layer-locked anomalous valley Hall effect in a two-dimensional A-type tetragonal antiferromagnetic insulator, *Phys. Rev. B* **109**, 134426 (2024).
 - [36] R. Van Haren, N. Hald, and D. Lederman, Emergent magnetic phases and piezomagnetic effects in Mn_xNi_{1-x}F₂ thin film alloys, *Phys. Rev. B* **108**, 134437 (2023).
 - [37] M. Jaime, A. Saul, M. Salamon, V. S. Zapf, N. Harrison, T. Durakiewicz, J. C. Lashley, D. A. Andersson, C. R. Stanek, J. L. Smith, and K. Gofryk, Piezomagnetism and magnetoelastic memory in uranium dioxide, *Nat. Commun* **8**, 99 (2017).
 - [38] H. Y. Ma, M. Hu, N. Li, J. Liu, W. Yao, J. F. Jia, and J. Liu, Multifunctional antiferromagnetic materials with giant piezomagnetism and noncollinear spin current, *Nat. Commun* **12**, 2846 (2021).
 - [39] Y. Zhu, T. Chen, Y. Li, L. Qiao, X. Ma, C. Liu, T. Hu, H. Gao, and W. Ren, Multipiezo Effect in Altermagnetic

- V₂SeTeO Monolayer, *Nano Lett* **24**, 472 (2023).
- [40] G. Kresse and J. Hafner, Ab initio molecular-dynamics simulation of the liquid-metal–amorphous-semiconductor transition in germanium, *Phys. Rev. B* **49**, 14251 (1994).
 - [41] P. E. Blöchl, Projector augmented-wave method, *Phys. Rev. B* **50**, 17953 (1994).
 - [42] G. Kresse and J. Furthmüller, Efficient iterative schemes for ab initio total-energy calculations using a plane-wave basis set, *Phys. Rev. B* **54**, 11169 (1996).
 - [43] J. P. Perdew, K. Burke, and M. Ernzerhof, Generalized gradient approximation made simple, *Phys. Rev. Lett.* **77**, 3865 (1996).
 - [44] P. J. Guo, Z. X. Liu, and Z. Y. Lu, Quantum anomalous hall effect in collinear antiferromagnetism, *NPJ Comput. Mater* **9**, 70 (2023).
 - [45] T. Zhao, S. Xing, J. Zhou, N. Miao, and Z. Sun, Stacking order modulated anomalous valley hall effect in antiferromagnetic mxene, *J. Materiomics* **10**, 269 (2024).
 - [46] A. Togo, F. Oba, and I. Tanaka, First-principles calculations of the ferroelastic transition between rutile-type and CaCl₂-type SiO₂ at high pressures, *Phys. Rev. B* **78**, 134106 (2008).
 - [47] Y. Niu, H. Lv, X. Wu, and J. Yang, Electric-field control of spin polarization above room temperature in single-layer a-type antiferromagnetic semiconductor, *J. Phys. Chem. Lett* **14**, 4042 (2023).
 - [48] Y. Qi, C. Yao, J. Zhao, and H. Zeng, Strain-induced tunable valley polarization and topological phase transition in svsn₂ monolayer, *J. Mater. Chem. C* **12**, 4417 (2024).
 - [49] C. Li and Y. An, Two-dimensional rare-earth Janus 2H–GdXY ($X, Y = \text{Cl, Br, I}; X \neq Y$) monolayers: Bipolar ferromagnetic semiconductors with high Curie temperature and large valley polarization, *Phys. Rev. B* **107**, 115428 (2023).
 - [50] Y. Wu, J. Tong, L. Deng, F. Luo, F. Tian, G. Qin, and X. Zhang, Coexisting ferroelectric and ferrovalley polarizations in bilayer stacked magnetic semiconductors, *Nano Lett* **23**, 6226 (2023).
 - [51] R.-W. Zhang, C. Cui, R. Li, J. Duan, L. Li, Z.-M. Yu, and Y. Yao, Predictable gate-field control of spin in alternemagnets with spin-layer coupling, *Phys. Rev. Lett.* **133**, 056401 (2024).